Performance Analysis of Ambient Backscatter Uplink NOMA Networks

Athanasios P. Chrysologou [1], Nestor D. Chatzidiamantis [1], Alexandros-Apostolos A. Boulogeorgos [2] and George K. Karagiannidis [1]

[1]Department of Electrical and Computer Engineering, Aristotle University of Thessaloniki, 54124 Thessaloniki, Greece.
E-mails: chrysolog@ece.auth.gr, nestoras@auth.gr, geokarag@auth.gr.
[2]Department of Electrical and Computer Engineering, University of Western Macedonia, 50100 Kozani, Greece.
E-mails: al.boulogeorgos@ieee.org.

2023 IEEE 97th Vehicular Technology Conference (VTC2023-Spring) | 979-8-3503-1114-3/23/$31.00 ©2023 IEEE | DOI: 10.1109/VTC2023-Spring57618.2023.10200724

***Abstract*—A core vision of the future sixth-generation wireless networks is to serve, in the most spectral and energy efficient way, a massive number of devices and/or Internet-of-Things (IoT) sensors, plenty of which are expected to be low-powered or even battery-free. In this direction, non-orthogonal multiple access (NOMA) and ambient backscatter communications (AmBC) are considered as two key promising technologies. In this work, we present a novel analytical framework for studying the performance of uplink NOMA-based AmBC systems. Specifically, analytical expressions for both NOMA-users' and IoT backscatter device's (BD) outage probabilities (OPs) are derived under both perfect and the more realistic case of imperfect successive interference cancellation (SIC). Likewise, system's performance at the high signal-to-noise ratio (SNR) regime is investigated as well as expressions for the system's overall average throughput are also derived. A performance comparison between the proposed setup and a conventional orthogonal multiple access (OMA)-based AmBC system is provided as well as it is proved that the proposed system's average throughput is equal or even greater compared to a conventional uplink NOMA system with two NOMA-users and no BDs.**

***Index Terms*—Ambient backscatter communications, non-orthogonal multiple access, imperfect successive interference cancellation, Internet-of-Things, outage probability.**

I. Introduction

As Ericsson predicts, by 2024 more than 22 billion Internet-of-Things (IoT) devices, with plenty of heterogeneous demands, different quality of experience (QoE) needs and various energy requirements, will be deployed globally [1]. This huge number makes the need of massive connectivity as well as of spectral and energy efficiency more timely than ever.

In this direction, multiple access techniques have proved to be a key promising technology for the support of massive connectivity [2]. Specifically, non-orthogonal multiple access (NOMA) allows plenty of devices to be served simultaneously in the most spectral efficient way since they share the same frequency, time or even code resources [3].

In the meantime, apart from the classical non-energy constrained communication scenarios, the next-generation-Internet-of-Things (NGIoT) vision is to also support energy constrained devices [4]. In this direction, ambient backscatter communications (AmBC) have been proposed and investigated by both academia and industry. In a typical AmBC scenario, the so-called backscatter devices (BDs) remodulate and reflect incident already-existing radio frequency signals (e.g., cellular or WiFi signals) by changing their antenna impedance [5].

Recently, all the above mentioned advantages have led to an increased research interest in the combination of AmBC with NOMA. In [6], a backscatter-NOMA scheme for a system setup with two downlink cellular users and a passive IoT device was proposed and investigated, while in [7], and in [8] a joint transmit power and reflection coefficient optimization framework and an energy efficiency maximization, respectively, were provided for a similar setup with [6]. Furthermore, [9] provided an effective capacity analysis for a typical downlink NOMA AmBC scenario and proved that increased reflection coefficient at BD leads to increased effective capacity for BD but decreased effective capacities for the NOMA-users. Moreover, in [10], and in [11], the outage and the ergodic capacity (EC) performance, respectively, of a downlink NOMA-based AmBC system model, where a source multiplexes two different messages for a single receiver, was investigated. In [12], a symbiotic AmBC framework, which consisted of one primary and one backscatter system, was presented and investigated in terms of EC and coexistence outage probability (COP). In [13], an uplink throughput maximization problem was formulated and solved in a communication scenario with one downlink user and multiple uplink BDs, while, in [14], a comparison, in terms of users' outage probability (OP) and EC, between backscatter communication assisted NOMA and wireless power transfer (WPT) assisted NOMA networks, was held. Finally, [15], [16], and [17] focused their analysis on the physical layer security (PLS) of downlink NOMA-AmBC networks. More specifically, [15] provided a secrecy analysis of such systems under I/Q imbalance, while [16] derived users' OPs and intercept probabilities (IPs) for such system models under both residual hardware impairments and channel estimation errors. In [17], Li *et al.* introduced a cognitive radio inspired AmBC setup and investigated its security and reliability by deriving users' OPs and IPs.

From the above discussions, it becomes evident that the great majority of the existing literature focuses on either downlink NOMA-assisted AmBC system setups or point-to-point communication setups under the coexistence of one or multiple BDs, thus, leaving the combination of uplink cellular and AmBC networks relatively unexplored.

Recognizing this gap, in this work we provide a novel analytical framework for investigating the reliability of uplink cellular networks that are able to support AmBC. More

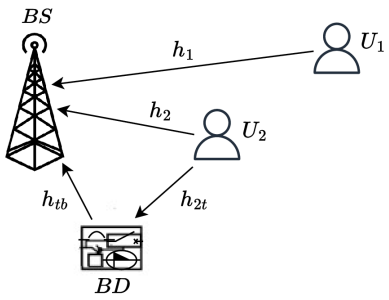

Fig. 1: System model.

specifically, the contributions of this work can be summarized as follows. A system setup that occurs from the integration of AmBC in NOMA-enabled uplink cellular networks is presented and investigated in terms of both NOMA-users' and BD's OPs. In comparison with the great majority of the existing works that assume perfect successive interference cancellation (pSIC), in this work, the aforementioned OPs are derived under both pSIC and the more realistic case of imperfect successive interference cancellation (ipSIC). Useful insights for the performance of the proposed system at the high signal-to-noise ratio (SNR) regime are obtained by evaluating NOMA-users' and BD's diversity orders and system's average throughput is also derived. A comparison, in terms of outage performance, between the proposed setup and a conventional orthogonal multiple access (OMA)-based AmBC system is provided as well as it is proved that despite the enhanced interference levels due to the coexistence of a BD, proposed system's average throughput is greater compared to a conventional uplink NOMA system with NOMA-users and no BDs.

II. System model

As depicted in Fig. 1, an uplink NOMA-based AmBC system setup is considered, which consists of a far-cellular user (U_1), a near-cellular user (U_2) and an IoT battery-free BD. Users U_1, U_2 intent to transmit their messages to the base station (BS) exploiting uplink NOMA, while BD takes advantage of the undergoing transmissions in order to also transmit its message to the BS over U_2's message. It is assumed that all nodes are equipped with a single antenna and the half-duplex mode of operation is considered.

The channels from U_1, U_2 to the BS are denoted as h_1, h_2 respectively, while the channels between U_2, BD and BD, BS are denoted as h_{2t} and h_{tb}, respectively. The direct link between U_1 and BD is considered negligible since the distance between these nodes is considered relatively large. All channels are assumed to be subject to Rayleigh fading plus additive white Gaussian noise (AWGN) with zero mean and variance N_0. Hence, the channel coefficients are denoted by $h_i \sim CN(0, \lambda_i)$ with $i \in \{1, 2, 2t, tb\}$. Furthermore, without loss of generality, the distance between U_2 and BS is considered shorter than the distance between U_1 and BS.

Following the uplink NOMA principle, U_1, U_2 simultaneously transmit their messages, x_1, x_2, respectively, to the BS. In the meantime, BD, which symbiotically coexists in the network, takes advantage of the undergoing transmissions and backscatters x_2 to the BS with its own message x_t. Hence, the signal received from BS can be modeled as follows:

$$y_{BS} = \sqrt{P}h_1x_1 + \sqrt{P}h_2x_2 + \sqrt{\eta P}h_{2t}h_{tb}x_2x_t + n_b, \quad (1)$$

where P is cellular users' transmit power, η denotes the BD's reflection coefficient with $0 \leq \eta \leq 1$ [13] and n_b is the AWGN coefficient at the BS.

According to the fact that in uplink NOMA is crucial to maintain the distinctness of received signals [18] and given the double-fading effect in BD's cascade channel as well as the generally small η value [9], the decoding order at the BS is considered as (x_2, x_1, x_t). Thus, the received signal-to-interference-plus-noise ratios (SINRs) at the BS for the decoding of all messages, considering ipSIC, can be given as follows:

$$\gamma_{x_2} = \frac{\rho|h_2|^2}{\rho|h_1|^2 + \eta\rho|h_{2t}|^2|h_{tb}|^2 + 1}, \quad (2)$$

$$\gamma_{x_1} = \frac{\rho|h_1|^2}{\eta\rho|h_{2t}|^2|h_{tb}|^2 + \rho|g_2|^2 + 1}, \quad (3)$$

$$\gamma_{x_t} = \frac{\eta\rho|h_{2t}|^2|h_{tb}|^2}{\rho|g_1|^2 + \rho|g_2|^2 + 1}, \quad (4)$$

where $\rho = \frac{P}{N_0}$ is users' transmit SNR, $g_1 \sim CN(0, k_1\lambda_1)$, $g_2 \sim \mathrm{CN}(0, k_2\lambda_2)$ with parameters k_1, k_2 denoting the impact of ipSIC. It is noted that for $j \in \{1, 2\}$ it holds $0 \leq k_j \leq 1$, where the case $k_j = 0$ refers to pSIC, whereas the case $k_j = 1$ refers to no SIC.

III. Performance Analysis

Assume that users transmit with constant data rates R_m, with $m \in \{1, 2, t\}$, in order to meet their required quality of service (QoS). In this case, OP becomes a meaningful performance evaluation criterion. In this section, exact closed-form expressions for the OPs of all messages in the proposed setup are derived. Furthermore, useful insights for U_1's, U_2's and BD's outage performance at the high SNR regime are provided and system's average throughput is also derived.

A. Outage performance of U_2

An outage for U_2 occurs only if the interference from U_1's and BD's messages combined with the AWGN at the BS do not allow the decoding of x_2. Hence U_2's OP can be given as

$$P_2^o = \Pr\left(\gamma_{x_2} < u_2\right), \quad (5)$$

where $u_2 = 2^{R_2} - 1$ is the SINR threshold for successful decoding of x_2. At this point, it is noted that ipSIC does not affect U_2's OP since message x_2 is decoded first at the BS.

The following theorem provides the OP of U_2.

Theorem 1. *The OP of U_2 can be evaluated as*

$$P_2^o = 1 - \frac{\lambda_2\sqrt{\lambda_2}e^{\frac{\lambda_2}{2u_2\eta\lambda_{2t}\lambda_{tb}} - \frac{u_2}{\lambda_2\rho}}}{(\lambda_2 + \lambda_1u_2)\sqrt{u_2\eta\lambda_{2t}\lambda_{tb}}}W_{-\frac{1}{2},0}\left(\frac{\lambda_2}{u_2\eta\lambda_{2t}\lambda_{tb}}\right), \quad (6)$$

where $W_{b,c}(\cdot)$ is the Whittaker function [19, (9.220.4)].

Proof: Applying (2) in (5), we get

$$P_2^o = \Pr\left(|h_2|^2 < |h_1|^2 u_2 + \eta Z u_2 + \frac{u_2}{\rho}\right), \quad (7)$$

where $Z = |h_{2t}|^2 |h_{tb}|^2$. It is noted that $|h_1|^2$, $|h_2|^2$ are exponentially distributed random variables, thus, $f_{|h_j|^2}(x) = \frac{1}{\lambda_j} e^{-\frac{x}{\lambda_j}}$ with $j \in \{1, 2\}$, where $f_X(\cdot)$ denotes the probability density function (PDF) of a random variable X. Furthermore, Z occurs as the product of two exponentially distributed random variables and its PDF is given as [6] $f_Z(z) = \frac{2}{\lambda_{2t}\lambda_{tb}} K_0\left(2\sqrt{\frac{z}{\lambda_{2t}\lambda_{tb}}}\right)$, where $K_0(\cdot)$ denotes the zero order modified Bessel function of the second kind. Considering that $|h_1|^2$, $|h_2|^2$, Z are independent with each other, (7) becomes

$$\begin{aligned} P_2^o &= \int_0^\infty f_Z(z) \int_0^\infty f_{|h_1|^2}(y) \\ &\quad \times \int_0^{y u_2 + \eta z u_2 + \frac{u_2}{\rho}} f_{|h_2|^2}(x)\, \mathrm{d}x\, \mathrm{d}y\, \mathrm{d}z \\ &= 1 - I_1, \end{aligned} \quad (8)$$

where

$$I_1 = \int_0^\infty f_Z(z) \int_0^\infty e^{-\frac{\rho y u_2 + \eta \rho z u_2 + u_2}{\lambda_2 \rho}} f_{|h_1|^2}(y)\, \mathrm{d}y\, \mathrm{d}z. \quad (9)$$

By substituting $f_{|h_1|^2}(y)$, $f_Z(z)$ in (9), it occurs

$$\begin{aligned} I_1 &= \frac{1}{\lambda_1} e^{-\frac{u_2}{\lambda_2 \rho}} \int_0^\infty \frac{2}{\lambda_{2t}\lambda_{tb}} K_0\left(2\sqrt{\frac{z}{\lambda_{2t}\lambda_{tb}}}\right) e^{-\frac{u_2 \eta z}{\lambda_2}}\, \mathrm{d}z \\ &\quad \times \int_0^\infty e^{-\frac{y}{\lambda_1}} e^{-\frac{u_2 y}{\lambda_2}}\, \mathrm{d}y \\ &= \frac{\lambda_2 e^{-\frac{u_2}{\lambda_2 \rho}}}{u_2\lambda_1 + \lambda_2} \int_0^\infty \frac{2}{\lambda_{2t}\lambda_{tb}} K_0\left(2\sqrt{\frac{z}{\lambda_{2t}\lambda_{tb}}}\right) e^{-\frac{u_2 \eta z}{\lambda_2}}\, \mathrm{d}z \\ &\overset{(s_1)}{=} \frac{\lambda_2 e^{-\frac{u_2}{\lambda_2 \rho}}}{u_2\lambda_1 + \lambda_2} \frac{\sqrt{\lambda_2} e^{\frac{\lambda_2}{2 u_2 \eta \lambda_{2t} \lambda_{tb}}}}{\sqrt{u_2 \eta \lambda_{2t} \lambda_{tb}}} W_{-\frac{1}{2},0}\left(\frac{\lambda_2}{u_2 \eta \lambda_{2t} \lambda_{tb}}\right), \end{aligned} \quad (10)$$

where step (s_1) comes from [19, (6.614.4)] and some straightforward algebraic manipulations. By invoking (10) in (8), we get (6) and this completes the proof. ∎

B. Outage performance of U_1

In order to avoid outage for x_1, BS must firstly decode x_2 and then attempt to decode x_1 via SIC. Hence, U_1's OP can be given as

$$P_1^o = 1 - \Pr\left(\gamma_{x_2} > u_2, \gamma_{x_1} > u_1\right), \quad (11)$$

where $u_1 = 2^{R_1} - 1$.

From the following theorem, a closed-form expression for U_1's OP can be obtained.

Theorem 2. *The closed-form expression for the OP of U_1 under ipSIC can be given by (12), while under pSIC can be given again by (12) as soon as k_2 is set equal to zero.*

$$P_1^o = 1 - \frac{\sqrt{\bar{A}} \lambda_1 \lambda_2 e^{-\frac{u_2}{\rho\lambda_2} - (\frac{1}{\lambda_1} + \frac{u_2}{\lambda_2})\frac{u_1}{\rho} + \frac{\bar{A}}{2}} W_{-\frac{1}{2},0}\left(\bar{A}\right)}{(\lambda_2 + u_2\lambda_1)(\lambda_1 + k_2 u_1 \lambda_2 + \lambda_1 k_2 u_1 u_2)}, \quad (12)$$

where $\bar{A} = \lambda_1\lambda_2(\lambda_{2t}\lambda_{tb}\eta)^{-1}(\lambda_1 u_2 + \lambda_2 u_1 + \lambda_1 u_1 u_2)^{-1}$.

Proof: Applying (2) and (3) in (11), we get

$$\begin{aligned} P_1^o &= 1 - \Pr\left(|h_2|^2 > |h_1|^2 u_2 + \eta Z u_2 + \frac{u_2}{\rho}, \right. \\ &\qquad \left. |h_1|^2 > \eta Z u_1 + |g_2|^2 u_1 + \frac{u_1}{\rho}\right) \\ &= 1 - \int_0^\infty f_{|g_2|^2}(w) \int_0^\infty f_Z(z) \int_{\eta z u_1 + w u_1 + \frac{u_1}{\rho}}^\infty f_{|h_1|^2}(y) \\ &\quad \times \int_{y u_2 + \eta z u_2 + \frac{u_2}{\rho}}^\infty f_{|h_2|^2}(x)\, \mathrm{d}x\, \mathrm{d}y\, \mathrm{d}z\, \mathrm{d}w \\ &= 1 - \frac{\lambda_1\lambda_2 e^{-\frac{u_2}{\rho\lambda_2} - (\frac{1}{\lambda_1} + \frac{u_2}{\lambda_2})\frac{u_1}{\rho}}}{(\lambda_1 + k_2 u_1 \lambda_2 + \lambda_1 k_2 u_1 u_2)(\lambda_2 + u_2\lambda_1)} \\ &\quad \times \int_0^\infty \frac{2}{\lambda_{2t}\lambda_{tb}} K_0\left(2\sqrt{\frac{z}{\lambda_{2t}\lambda_{tb}}}\right) e^{-z(\frac{u_2\eta}{\lambda_2} + \frac{u_1\eta}{\lambda_1} + \frac{u_1 u_2 \eta}{\lambda_2})}\mathrm{d}z. \end{aligned} \quad (13)$$

By invoking [19, (6.614.4)] in (13), we get (12).

In case of pSIC, the extraction of U_1's OP is updated as

$$\begin{aligned} P_1^{o,\ pSIC} &= 1 - \Pr\left(|h_2|^2 > |h_1|^2 u_2 + \eta Z u_2 + \frac{u_2}{\rho}, \right. \\ &\qquad \left. |h_1|^2 > \eta Z u_1 + \frac{u_1}{\rho}\right). \end{aligned} \quad (14)$$

By following similar lines with the case of ipSIC, it can be proved that (14) becomes equal to (13) as soon as k_2 is set equal to zero. This completes the proof. ∎

C. Outage performance of BD

For the successful decoding of x_t, BS must firstly decode x_2 and x_1 and then attempt to decode x_t via SIC. Thus,

$$P_t^o = 1 - \Pr\left(\gamma_{x_2} > u_2, \gamma_{x_1} > u_1, \gamma_{x_t} > u_t\right), \quad (15)$$

where $u_t = 2^{R_t} - 1$.

In what follows, we provide a theorem that returns BD's OP under three different cases, namely C-I) the elimination of x_2 during SIC is perfect, while the elimination of x_1 during SIC is imperfect, i.e., arbitrary k_1, while $k_2 = 0$ is assumed, C-II) the elimination of x_2 during SIC is imperfect, while the elimination of x_1 during SIC is perfect, i.e., arbitrary k_2, while $k_1 = 0$ is assumed[1] and C-III) pSIC is assumed, thus both x_1, x_2 are perfectly eliminated during SIC, i.e., $k_1 = k_2 = 0$.

Theorem 3. *The OP of the BD for cases C-I and C-II can be obtained via (17) by setting $j = 1$ and $j = 2$, respectively, while for the case of pSIC can be obtained via (18) given at the top of the next page, where* $A = \frac{2\lambda_2 e^{-\frac{u_2}{\rho\lambda_2} - (\frac{1}{\lambda_1} + \frac{u_2}{\lambda_2})\frac{u_1}{\rho}}}{\lambda_{2t}\lambda_{tb}(\lambda_2 + \lambda_1 u_2)}$, $B = \frac{u_2\eta}{\lambda_2}(1 + u_1) + \frac{u_1\eta}{\lambda_1}$, $\psi_n = \cos(\frac{\pi(2n-1)}{2M})$, $\psi_i = \cos(\frac{\pi(2i-1)}{2N})$, $\psi_l = \cos(\frac{\pi(2l-1)}{2Q})$ *with M, N and Q being accuracy-complexity trade-off parameters,*

$$\tilde{q} = \begin{cases} \frac{1}{k_1\lambda_1}, & \textit{case C-I} \\ \frac{1}{k_2\lambda_2} + \frac{u_1 u_2}{\lambda_2} + \frac{u_1}{\lambda_1}, & \textit{case C-II} \end{cases} \quad (16)$$

and $a_1 = B\lambda_{2t}\lambda_{tb} + \frac{\tilde{q}\lambda_{2t}\lambda_{tb}\eta}{u_t(\psi_n + 1)}$.

[1] A similar ipSIC model with C-II was used in [20].

$$P_t^o \approx 1 - A\left(\frac{\sqrt{\lambda_{2t}\lambda_{tb}}e^{\frac{1}{2B\lambda_{2t}\lambda_{tb}}}}{2\sqrt{B}}W_{-\frac{1}{2},0}\left(\frac{1}{B\lambda_{2t}\lambda_{tb}}\right)\frac{1}{k_j\lambda_j\tilde{q}} - \frac{2\pi\eta(\lambda_{2t}\lambda_{tb})^2 e^{\frac{\tilde{q}}{\rho}}}{k_j\lambda_j u_t M}\sum_{n=1}^{M}\frac{\sqrt{1-\psi_n^2}}{(\psi_n+1)^2}\left(\frac{a_1^{-\frac{3}{2}}e^{\frac{1}{2a_1}}}{2}W_{-\frac{3}{2},0}\left(\frac{1}{a_1}\right)\right.\right.$$
$$\left.\left. - \frac{\pi u_t(\psi_n+1)}{4N\lambda_{2t}\lambda_{tb}\eta\rho}\sum_{i=1}^{N}\sqrt{1-\psi_i^2}\frac{u_t(\psi_n+1)(\psi_i+1)}{4\lambda_{2t}\lambda_{tb}\eta\rho}e^{-\frac{a_1 u_t(\psi_n+1)(\psi_i+1)}{4\lambda_{2t}\lambda_{tb}\eta\rho}}K_o\left(2\sqrt{\frac{u_t(\psi_n+1)(\psi_i+1)}{4\lambda_{2t}\lambda_{tb}\eta\rho}}\right)\right)\right), \tag{17}$$

$$P_t^{o,\ pSIC} \approx 1 - \frac{A\sqrt{\lambda_{2t}\lambda_{tb}}e^{\frac{1}{2B\lambda_{2t}\lambda_{tb}}}}{2\sqrt{B}}W_{-\frac{1}{2},0}\left(\frac{1}{B\lambda_{2t}\lambda_{tb}}\right) + \frac{A\pi u_t}{2\eta\rho Q}\sum_{l=1}^{Q}\sqrt{1-\psi_l^2}K_o\left(2\sqrt{\frac{u_t(\psi_l+1)}{2\lambda_{2t}\lambda_{tb}\eta\rho}}\right)e^{-\frac{Bu_t(\psi_l+1)}{2\eta\rho}} \tag{18}$$

Proof: For the case C-I, by substituting (2), (3) and (4) in (15), it occurs

$$\begin{aligned}P_t^{o,I} &= 1 - \Pr\left(|h_2|^2 > |h_1|^2 u_2 + \eta Z u_2 + \frac{u_2}{\rho},\right.\\ &\quad \left.|h_1|^2 > \eta Z u_1 + \frac{u_1}{\rho},\ Z > \frac{u_t|g_1|^2}{\eta} + \frac{u_t}{\eta\rho}\right)\\ &= 1 - \int_0^\infty f_{|g_1|^2}(w)\int_{\frac{u_t w}{\eta}+\frac{u_t}{\eta\rho}}^\infty f_Z(z)\int_{\eta z u_1+\frac{u_1}{\rho}}^\infty f_{|h_1|^2}(y)\\ &\quad \times \int_{yu_2+\eta z u_2+\frac{u_2}{\rho}}^\infty f_{|h_2|^2}(x)\,\mathrm{d}x\,\mathrm{d}y\,\mathrm{d}z\,\mathrm{d}w\\ &\overset{(s_2)}{=} 1 - A\int_0^\infty f_{|g_1|^2}(w)\\ &\quad \times \underbrace{\int_{\frac{u_t w}{\eta}+\frac{u_t}{\eta\rho}}^\infty K_0\left(2\sqrt{\frac{z}{\lambda_{2t}\lambda_{tb}}}\right)e^{-Bz}\,\mathrm{d}z\,\mathrm{d}w}_{I_2},\end{aligned} \tag{19}$$

where step (s_2) can be obtained by following similar steps with the proofs of theorems 1, 2.

Concerning I_2, it can be calculated as follows

$$\begin{aligned}I_2 &= \int_0^\infty K_0\left(2\sqrt{\frac{z}{\lambda_{2t}\lambda_{tb}}}\right)e^{-Bz}\mathrm{d}z\\ &\quad - \int_0^{\frac{u_t w}{\eta}+\frac{u_t}{\eta\rho}} K_0\left(2\sqrt{\frac{z}{\lambda_{2t}\lambda_{tb}}}\right)e^{-Bz}\mathrm{d}z\\ &\triangleq I_{21} - I_{22}.\end{aligned} \tag{20}$$

Integral I_{21} can be calculated via [19, (6.614.4)] as

$$I_{21} = \frac{\sqrt{\lambda_{2t}\lambda_{tb}}e^{\frac{1}{2B\lambda_{2t}\lambda_{tb}}}}{2\sqrt{B}}W_{-\frac{1}{2},0}\left(\frac{1}{B\lambda_{2t}\lambda_{tb}}\right). \tag{21}$$

On the other hand, to the best of authors' knowledge, I_{22} cannot be obtained in a closed form. However, applying the well-known Chebyshev-Gaussian quadrature, we get

$$\begin{aligned}I_{22} &\approx \frac{\pi(u_t+u_t\rho w)}{2\eta\rho M}\sum_{n=1}^{M}\sqrt{1-\psi_n^2}\,e^{-B\frac{(u_t+u_t\rho w)(\psi_n+1)}{2\eta\rho}}\\ &\quad \times K_o\left(2\sqrt{\frac{(u_t+u_t\rho w)(\psi_n+1)}{2\lambda_{2t}\lambda_{tb}\eta\rho}}\right).\end{aligned} \tag{22}$$

Hence, (19) becomes

$$\begin{aligned}P_t^{o,I} &= 1 - A\left(I_{21}\int_0^\infty f_{|g_1|^2}(w)\mathrm{d}w - \int_0^\infty I_{22}f_{|g_1|^2}(w)\mathrm{d}w\right)\\ &= 1 - A(I_{21} - I_3),\end{aligned} \tag{23}$$

where

$$I_3 = \int_0^\infty I_{22}f_{|g_1|^2}(w)\mathrm{d}w. \tag{24}$$

Invoking (22) in (24), I_3 becomes

$$\begin{aligned}I_3 &= \int_0^\infty \frac{e^{-\frac{w}{k_1\lambda_1}}}{k_1\lambda_1}\frac{\pi(u_t+u_t\rho w)}{2\eta\rho M}\sum_{n=1}^{M}e^{-B(\frac{u_t+u_t\rho w}{2\eta\rho}(\psi_n+1))}\\ &\quad \times K_o\left(2\sqrt{\frac{(u_t+u_t\rho w)(\psi_n+1)}{2\lambda_{2t}\lambda_{tb}\eta\rho}}\right)\sqrt{1-\psi_n^2}\,\mathrm{d}w.\end{aligned} \tag{25}$$

Next, I_3 will be calculated. By changing variable of $y = \frac{(u_t+u_t\rho w)(\psi_n+1)}{2\lambda_{2t}\lambda_{tb}\eta\rho}$, we get

$$I_3 = \frac{2\pi\eta(\lambda_{2t}\lambda_{tb})^2 e^{\frac{1}{\rho k_1\lambda_1}}}{k_1\lambda_1 u_t M}\sum_{n=1}^{M}\frac{\sqrt{1-\psi_n^2}}{(\psi_n+1)^2}\,I_{31}, \tag{26}$$

where

$$\begin{aligned}I_{31} &= \int_{\frac{u_t(\psi_n+1)}{2\lambda_{2t}\lambda_{tb}\eta\rho}}^\infty yK_0\left(2\sqrt{y}\right)e^{-y(B\lambda_{2t}\lambda_{tb}+\frac{2\eta\lambda_{2t}\lambda_{tb}}{k_1\lambda_1 u_t(\psi_n+1)})}\mathrm{d}y\\ &= \int_0^\infty yK_0\left(2\sqrt{y}\right)e^{-y(B\lambda_{2t}\lambda_{tb}+\frac{2\eta\lambda_{2t}\lambda_{tb}}{k_1\lambda_1 u_t(\psi_n+1)})}\mathrm{d}y\\ &\quad - \int_0^{\frac{u_t(\psi_n+1)}{2\lambda_{2t}\lambda_{tb}\eta\rho}} yK_0\left(2\sqrt{y}\right)e^{-y(B\lambda_{2t}\lambda_{tb}+\frac{2\eta\lambda_{2t}\lambda_{tb}}{k_1\lambda_1 u_t(\psi_n+1)})}\mathrm{d}y.\end{aligned} \tag{27}$$

The first integral of (27) can be calculated via [19, (6.643.3)]. On the other hand, to the best of authors' knowledge, the second integral of (27) cannot be calculated in a closed-form. However, it can be approximated using the Chebyshev-Gaussian quadrature. Hence, (27) becomes

$$\begin{aligned}I_{31} &\approx \frac{a_1^{-\frac{3}{2}}e^{\frac{1}{2a_1}}}{2}W_{-\frac{3}{2},0}\left(\frac{1}{a_1}\right) - \frac{\pi u_t(\psi_n+1)}{4N\lambda_{2t}\lambda_{tb}\eta\rho}\sum_{i=1}^{N}\sqrt{1-\psi_i^2}\\ &\quad \times K_o\left(2\sqrt{\frac{u_t(\psi_n+1)(\psi_i+1)}{4\lambda_{2t}\lambda_{tb}\eta\rho}}\right)e^{-\frac{a_1 u_t(\psi_n+1)(\psi_i+1)}{4\lambda_{2t}\lambda_{tb}\eta\rho}}\\ &\quad \times \frac{u_t(\psi_n+1)(\psi_i+1)}{4\lambda_{2t}\lambda_{tb}\eta\rho},\end{aligned} \tag{28}$$

where $a_1 = B\lambda_{2t}\lambda_{tb} + \frac{2\eta\lambda_{2t}\lambda_{tb}}{k_1\lambda_1 u_t(\psi_n+1)}$. At this point, by firstly invoking (28) in (26) and then the resultant (26) and (21) in (23), we get (17) when $j=1$ and $\tilde{q} = \frac{1}{k_1\lambda_1}$.

In terms of C-II, we must properly update (19) as follows

$$\begin{aligned} P_t^{o,II} &= 1 - \Pr\Bigg(|h_2|^2 > |h_1|^2 u_2 + \eta Z u_2 + \frac{u_2}{\rho}, \\ &\quad |h_1|^2 > \eta Z u_1 + |g_2|^2 u_1 + \frac{u_1}{\rho},\ Z > \frac{u_t|g_2|^2}{\eta} + \frac{u_t}{\eta\rho}\Bigg) \\ &\overset{(s_3)}{=} 1 - A\int_0^{\infty} f_{|g_2|^2}(w)\, e^{-(\frac{u_1 u_2}{\lambda_2} + \frac{u_1}{\lambda_1})w} \\ &\quad \times \int_{\frac{u_t w}{\eta} + \frac{u_t}{\eta\rho}}^{\infty} K_0\left(2\sqrt{\frac{z}{\lambda_{2t}\lambda_{tb}}}\right) e^{-Bz}\, \mathrm{d}z\, \mathrm{d}w, \end{aligned} \tag{29}$$

where step (s_3) occurs by following similar lines with the extraction of (19). By evaluating the double integral of (29) in a similar manner with the one of (19), it occurs that $P_t^{o,II}$ can be given via (17) as soon as $j=2$ and $\tilde{q}$ is set equal to $\frac{1}{k_2\lambda_2} + \frac{u_1 u_2}{\lambda_2} + \frac{u_1}{\lambda_1}$.

For case C-III, i.e., the case of pSIC, unlike U_1's OP, but similarly with a lot of cases in the existing literature [21], BD's OP under pSIC cannot be evaluated by just setting $k_1 = k_2 = 0$ in (17). Hence, it is necessary we update BD's OP for the case of pSIC as follows

$$\begin{aligned} P_t^{o,\ pSIC} &= 1 - \Pr\Bigg(|h_2|^2 > |h_1|^2 u_2 + \eta Z u_2 + \frac{u_2}{\rho}, \\ &\quad |h_1|^2 > \eta Z u_1 + \frac{u_1}{\rho},\ Z > \frac{u_t}{\eta\rho}\Bigg). \end{aligned} \tag{30}$$

By calculating the above probability in similar manner with the probability of (19), it can be proved that $P_t^{o,\ pSIC}$ can be given via (18). This completes the proof. ∎

D. High SNR regime

When it comes for system's overall performance, the diversity order achieved by users is considered a useful insight.

By applying $e_{x\to 0}^{-x} \sim 1 - x$ and $K_0^{x\to 0}(x) \sim \ln(\frac{1}{x})$ in P_2^o, P_1^o, $P_t^{o,I}$, $P_t^{o,II}$, $P_1^{o,\ pSIC}$, $P_t^{o,\ pSIC}$ and by using diversity order's definition

$$d_m = -\lim_{\rho\to\infty}\frac{\log P_m^o(\rho)}{\log\rho}, \quad d_m^{pSIC} = -\lim_{\rho\to\infty}\frac{\log P_m^{o,\ pSIC}(\rho)}{\log\rho}, \tag{31}$$

for ipSIC and pSIC, respectively, it can be straightforwardly shown that NOMA-users' and BD's diversity orders are equal to zero in all cases, i.e., $d_m = d_m^{pSIC} = 0,\ m \in \{1,2,t\}$.

E. Throughput Analysis

Based on NOMA-users' and BD's OPs and target data rates, system's average throughput can be obtained as

$$\bar{T} = \sum_m (1 - P_m^o) R_m, \quad m \in \{1,2,t\}, \tag{32}$$

$$\bar{T}^{pSIC} = \sum_m (1 - P_m^{o,\ pSIC}) R_m, \quad m \in \{1,2,t\}, \tag{33}$$

for the cases of ipSIC and pSIC, respectively.

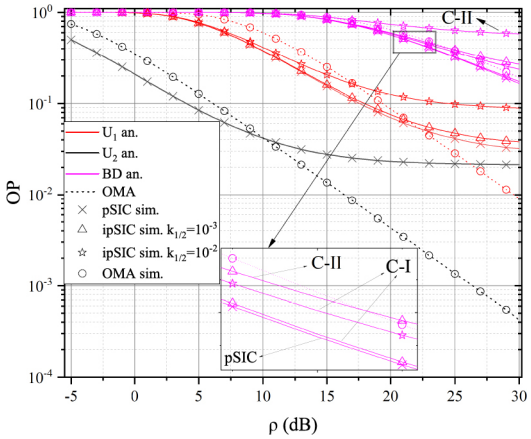

Fig. 2: OPs of U_1, U_2 and BD with respect to ρ for the proposed system setup and OMA.

IV. Numerical Results & Discussions

In this section, both simulations (sim.) and analytical (an.) results are provided in order to verify the presented analysis and to examine proposed (prop.) system model's outage performance versus different system parameters for both pSIC and ipSIC cases. For the extraction of Figs. 2-4, $\lambda_1 = 0.1$, $\lambda_2 = 1.5$. $\lambda_{2t} = 0.4$, $\lambda_{tb} = 0.4$, $M = N = Q = 15$ and $R_1 = 0.5$, $R_2 = 0.4$, $R_t = 0.1$ bps/Hz are considered. Furthermore, unless otherwise mentioned, $\eta = 0.01$ is assumed.

In Fig. 2, NOMA-users' and BD's OPs versus transmit SNR ρ are presented. Furthermore, an OMA scheme is also provided as benchmark. Analytical results coincide with simulation ones, thus the authenticity of the presented analysis is further validated. It is illustrated that U_2's OP for the proposed scheme outperforms OMA until ρ reaches 10 dBs and then OMA achieves lower OPs. On the other hand, in terms of U_1, NOMA outperforms OMA for the whole region of $\rho \in [-5, 22]$ dBs when pSIC or ipSIC with $k_2 = 0.001$ is applied. It is also interesting that even for the case of ipSIC with $k_2 = 0.01$, NOMA outperforms OMA at the low-to-medium SNR region. In terms of the BD, it can be observed that, under both pSIC or ipSIC case C-I with $k_1 = 0.001$, the proposed scheme outperforms OMA for the whole SNR region. Finally, it is shown that all U_1, U_2 and BD reach floors at high SNRs; thus, the analysis presented in section III-D is further validated.

In Fig. 3, NOMA-users' and BD's OP for the proposed scheme and versus reflection coefficient η, are illustrated when $\rho = 30$ dBs. It is obvious that as η increases, U_1's, U_2's OP also increases. This happens since, as (2) and (3) witness, increased η leads to increased interference during the decoding of x_1, x_2. On the other hand, BD's outage performance versus η shows a convex behavior, i.e., BS's OP decreases up to a specific η value and then begins to increase. This may seem contradictory since as η increases, the SINR γ_{x_t} also increases. However, as (15) witnesses, for the successful decoding of x_t it is also necessary that x_2, x_1 are also successfully decoded. Hence, the fact that increased η leads to increased γ_{x_t} but decreased γ_{x_1} and γ_{x_2} explains this convex behavior.

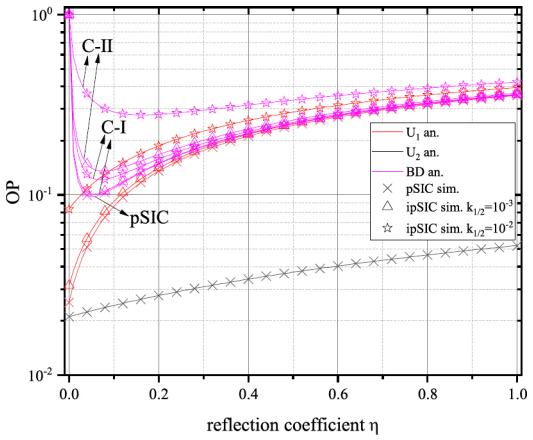

Fig. 3: OPs of U_1, U_2 and BD versus reflection coefficient η when $\rho = 30$ dBs for the proposed system setup.

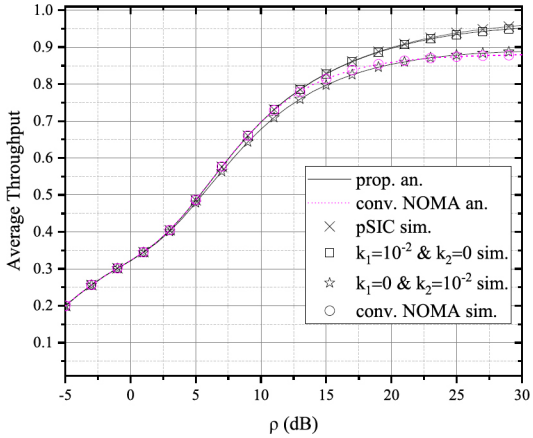

Fig. 4: System's average throughput for the proposed system setup and conventional NOMA.

Fig. 4 illustrates system's average throughput versus transmit SNR ρ. Except from the proposed NOMA scheme, a conventional uplink NOMA (conv. NOMA) scheme with 2 users and without any BDs, is also presented as a benchmark. Interestingly, the proposed scheme reaches the same performance or even outperforms conventional NOMA for the SNR region discussed. This means that system's overall throughput remains robust against the enhanced interference levels that the coexistence of a passive BD adds in the network.

V. Conclusion

In this work, an analytical framework for investigating the outage performance of uplink NOMA-AmBC networks was presented. Analytical expressions for the OPs of both NOMA-users and battery-free BD were derived for both pSIC and ipSIC cases as well as NOMA-users' and BD's diversity orders were evaluated for all cases. Numerical results revealed that the proposed NOMA-based setup leads to enhanced outage performance, compared to an OMA-AmBC system, for both NOMA-users and BD for the most of the practical transmit SNR values and also proved that the proposed setup outperforms a conventional uplink NOMA network with no BDs in terms of average throughput. As a future work, the PLS of the proposed uplink NOMA-AmBC system can be investigated.

References

[1] L. Ericsson, "Ericsson Mobility Report June 2020," *Ericsson*, vol. 36, pp. 1–36, 2020.

[2] Y. L. Lee, D. Qin, L.-C. Wang, and G. H. Sim, "6G massive radio access networks: Key applications, requirements and challenges," *IEEE Open J. Veh. Technol.*, vol. 2, pp. 54–66, Dec. 2020.

[3] Z. Ding, X. Lei, G. K. Karagiannidis, R. Schober, J. Yuan, and V. K. Bhargava, "A survey on non-orthogonal multiple access for 5G networks: Research challenges and future trends," *IEEE J. Sel. Areas Commun.*, vol. 35, no. 10, pp. 2181–2195, Oct. 2017.

[4] M. Brynskov, F. M. Facca, and G. Hrasko, "Next Generation Internet of Things," *H2020 Coordination and Support Action (CSA), NGIoT Consortium*, vol. 2021, p. 2019, 2018.

[5] R. Long, Y.-C. Liang, H. Guo, G. Yang, and R. Zhang, "Symbiotic radio: A new communication paradigm for passive Internet of Things," *IEEE Internet Things J.*, vol. 7, no. 2, pp. 1350–1363, Feb. 2020.

[6] Q. Zhang, L. Zhang, Y.-C. Liang, and P.-Y. Kam, "Backscatter-NOMA: A symbiotic system of cellular and Internet-of-Things networks," *IEEE Access*, vol. 7, pp. 20 000–20 013, Feb. 2019.

[7] W. U. Khan, X. Li, M. Zeng, and O. A. Dobre, "Backscatter-enabled NOMA for future 6G systems: A new optimization framework under imperfect SIC," *IEEE Commun. Lett.*, vol. 25, no. 5, pp. 1669–1672, May 2021.

[8] Y. Xu, Z. Qin, G. Gui, H. Gacanin, H. Sari, and F. Adachi, "Energy efficiency maximization in NOMA enabled backscatter communications with QoS guarantee," *IEEE Wireless Commun. Lett.*, vol. 10, no. 2, pp. 353–357, Feb. 2021.

[9] X. Li, H. Liu, G. Li, Y. Liu, M. Zeng, and Z. Ding, "Effective capacity analysis of AmBC-NOMA communication systems," *IEEE Trans. Veh. Technol.*, Oct. 2022.

[10] M. Elsayed, A. Samir, A. A. A. El-Banna, X. Li, and B. M. ElHalawany, "When NOMA multiplexing meets symbiotic ambient backscatter communication: Outage analysis," *IEEE Trans. Veh. Technol.*, vol. 71, no. 1, pp. 1026–1031, Jan. 2022.

[11] M. Elsayed, A. Samir, A. A. A. El-Banna, K. Rabie, X. Li, and B. M. ElHalawany, "Symbiotic Ambient Backscatter IoT Transmission over NOMA-enabled Network," in *Proc. IEEE Int. Conf. Commun. (ICC)*, Aug. 2022, pp. 2266–2271.

[12] H. Ding, M.-S. Alouini, K. Xin, H. Li, and S. Xu, "Symbiotic Ambient Backscatter Systems: Outage Behavior and Ergodic Capacity," *IEEE Internet Things J.*, Jul. 2022.

[13] Z. Ding and H. V. Poor, "On the application of BAC-NOMA to 6G umMTC," *IEEE Commun. Lett*, vol. 25, no. 8, pp. 2678–2682, Aug. 2021.

[14] Z. Ding, "Harvesting devices' heterogeneous energy profiles and QoS requirements in IoT: WPT-NOMA vs BAC-NOMA," *IEEE Trans. Commun*, vol. 69, no. 5, pp. 2837–2850, May 2021.

[15] X. Li, M. Zhao, Y. Liu, L. Li, Z. Ding, and A. Nallanathan, "Secrecy analysis of ambient backscatter NOMA systems under I/Q imbalance," *IEEE Trans. Veh. Technol.*, vol. 69, no. 10, pp. 12 286–12 290, Oct. 2020.

[16] X. Li, M. Zhao, M. Zeng, S. Mumtaz, V. G. Menon, Z. Ding, and O. A. Dobre, "Hardware impaired ambient backscatter NOMA systems: Reliability and Security," *IEEE Trans. Commun*, vol. 69, no. 4, pp. 2723–2736, Apr. 2021.

[17] X. Li, Y. Zheng, W. U. Khan, M. Zeng, D. Li, G. Ragesh, and L. Li, "Physical layer security of cognitive ambient backscatter communications for green Internet-of-Things," *IEEE Trans. Green Commun. Netw.*, vol. 5, no. 3, pp. 1066–1076, Sept. 2021.

[18] M. S. Ali, H. Tabassum, and E. Hossain, "Dynamic User Clustering and Power allocation for uplink and downlink non-orthogonal multiple access (NOMA) systems," *IEEE Access*, vol. 4, pp. 6325–6343, Aug. 2016.

[19] I. S. Gradshteyn and I. M. Ryzhik, *Table of integrals, series, and products*. Academic press, 2014.

[20] X. Yue and Y. Liu, "Performance analysis of intelligent reflecting surface assisted NOMA networks," *IEEE Trans. Wireless Commun.*, vol. 21, no. 4, pp. 2623–2636, Apr. 2022.

[21] A. P. Chrysologou, N. D. Chatzidiamantis, and G. K. Karagiannidis, "Cooperative Uplink NOMA in D2D Communications," *IEEE Commun. Lett.*, pp. 1–1, Aug. 2022.